ELSEVIER

Catalysis Today 79–80 (2003) 67–75

CATALYSIS TODAY

www.elsevier.com/locate/cattod

# Mass transfer in bubble columns

R. Krishna*, J.M. van Baten

*Department of Chemical Engineering, University of Amsterdam, Nieuwe Achtergracht 166, 1018 WV Amsterdam, The Netherlands*

**Abstract**

Bubble columns are operated either in the homogeneous or heterogeneous flow regime. In the homogeneous flow regime, the bubbles are nearly uniform in size and shape. In the heterogeneous flow regime, a distribution of bubble sizes exists. In this paper, a computational fluid dynamics (CFD) model is developed to describe the hydrodynamics, and mass transfer, of bubble columns operating in either of the two flow regimes. The heterogeneous flow regime is assumed to consist of two bubble classes: "small" and "large" bubbles. For the air–water system, appropriate drag relations are suggested for these two bubble classes.

Interactions between both bubble populations and the liquid are taken into account in terms of momentum exchange, or drag, coefficients, which differ for the "small" and "large" bubbles. The turbulence in the liquid phase is described using the $k$–$\varepsilon$ model.

For bubble columns operating with the air–water system, CFD simulations have been carried out for superficial gas velocities, $U$, in the range 0–0.08 m/s, spanning both regimes. These simulations reveal some of the characteristic features of homogeneous and heterogeneous flow regimes, and of regime transition on the gas holdup and mass transfer. By comparing the simulations with measured experimental data, it is concluded that mass transfer from the large bubble population is significantly enhanced due to frequent coalescence and break-up into smaller bubbles. The CFD simulations also underline the strong influence of column diameter on hydrodynamics and mass transfer.


*Keywords:* Bubble columns; Large bubbles; Small bubbles; Flow regimes; Bubble rise velocity; Mass transfer; Computational fluid dynamics

## 1. Introduction

When a column filled with a liquid is sparged with gas, the bed of liquid begins to expand as soon as gas is introduced. As the gas velocity is increased, the gas holdup $\varepsilon$ increases almost linearly with the superficial gas velocity, $U$, provided the value of $U$ stays below a certain value $U_{\text{trans}}$. This regime of operation of a bubble column is called the *homogeneous bubbly flow regime*. The bubble size distribution is narrow and a roughly uniform bubble size, generally in the range 1–7 mm, is found. When the superficial gas velocity $U$ reaches the value $U_{\text{trans}}$, coalescence of the bubbles takes place to produce the first fast-rising "large" bubble. The appearance of the first large bubble changes the hydrodynamic picture dramatically. The hydrodynamic picture in a gas–liquid system for velocities exceeding $U_{\text{trans}}$ is commonly referred to as the *heterogeneous* or *churn-turbulent flow regime* [1]. In the heterogeneous regime, small bubbles combine in clusters to form large bubbles in the size range 20–70 mm [2,3]. These large bubbles travel up through the column at high velocities (in the range 1–2 m/s), in a more or less plug flow manner [2].

* Corresponding author. Tel.: +31-20-525-7007; fax: +31-20-525-5604.
*E-mail address:* krishna@science.uva.nl (R. Krishna).

0920-5861/03/$ – see front matter © 2003 Elsevier Science B.V. All rights reserved.
doi:10.1016/S0920-5861(03)00046-4

**Nomenclature**

| | |
|---|---|
| $a$ | interfacial area per unit volume of dispersion ($m^2/m^3$) |
| $C_D$ | drag coefficient (dimensionless) |
| $C_G$ | gas phase concentration (arbitrary units) |
| $C_L$ | liquid phase concentration (arbitrary units) |
| $C_L^*$ | equilibrium liquid phase concentration (arbitrary units) |
| $d_b$ | diameter of bubble (m) |
| $Đ_k$ | diffusivity in phase $k$ (m) |
| $D_T$ | column diameter (m) |
| Eö | Eötvös number ($g(\rho_L - \rho_G)d_b^2/\sigma$) |
| $g$ | gravitational acceleration, 9.81 m/s$^2$ |
| $\boldsymbol{g}$ | gravitational vector (m/s$^2$) |
| $H$ | Henry coefficient (dimensionless) |
| $k_L$ | mass transfer coefficient in liquid phase (m/s) |
| $\boldsymbol{M}$ | interphase momentum exchange term (N/m$^3$) |
| $p$ | system pressure (Pa) |
| $r$ | radial coordinate (m) |
| $t$ | time (s) |
| $\boldsymbol{u}$ | velocity vector (m/s) |
| $U$ | superficial gas velocity in the riser (m/s) |
| $U_{trans}$ | regime transition velocity (m/s) |
| $V_L(0)$ | center-line liquid velocity (m/s) |
| $V_L(r)$ | radial distribution of liquid velocity (m/s) |
| $V_b$ | bubble rise velocity (m/s) |
| $V_{b0}$ | single bubble rise velocity (m/s) |

*Greek letters*

| | |
|---|---|
| $\varepsilon$ | total gas holdup (dimensionless) |
| $\mu$ | viscosity of fluid phase (Pa s) |
| $\rho$ | density of phase (kg/m$^3$) |
| $\sigma$ | surface tension of liquid phase (N/m) |

*Superscript*

| | |
|---|---|
| $*$ | equilibrium value |

*Subscripts*

| | |
|---|---|
| b | referring to bubbles |
| G | referring to gas |
| L | referring to liquid |
| T | tower or column |
| $k$, $l$ | referring to phases $k$ and $l$, respectively |
| trans | referring to the regime transition |

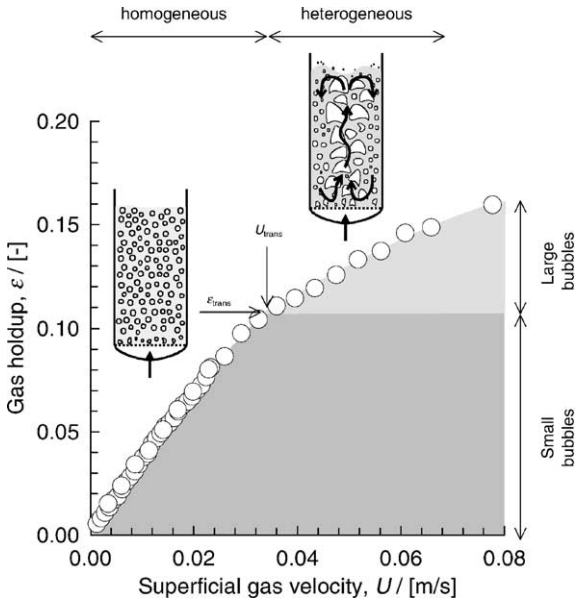


Fig. 1. Experimental data on gas holdup in a 0.1 m diameter bubble column operating with the air–water system spanning both the homogeneous and heterogeneous flow regimes.

These large bubbles have the effect of churning up the liquid phase and because of their high rise velocities they account for a major fraction of the gas throughput [4]. Small bubbles, which co-exist with large bubbles in the churn-turbulent regime, are "entrained" in the liquid phase and, as a good approximation, have the same back-mixing characteristics of the liquid phase. The two regimes are illustrated in Fig. 1, with experimental data for operation of a bubble column of 0.1 m diameter with the air–water system. We note a change in the slope in the $\varepsilon$–$U$ curve at the transition point.

Several recent publications have established the potential of computational fluid dynamics (CFD) for describing the hydrodynamics of bubble columns [5–16]. These CFD models are developed for either the homogeneous [7–10] or heterogeneous [11–16] flow regimes. However, none of the published CFD models have studied the interphase mass transfer in the two regimes. The major objective of the present communication is to develop a CFD model to describe both the hydrodynamics and mass transfer. The second objective is to examine the extent to which CFD models can be used to study the influence of column diameter on hydrodynamics and mass transfer.

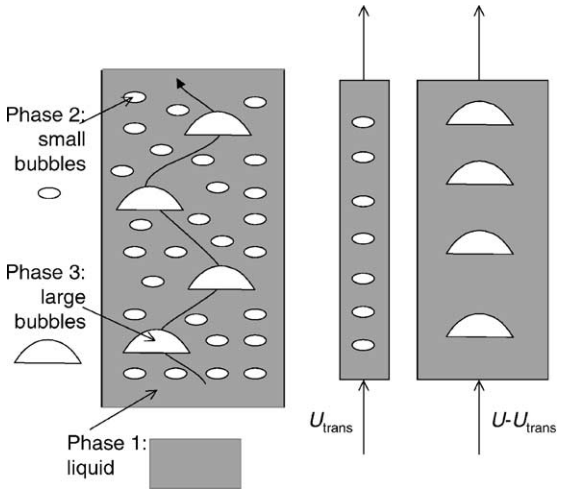


Fig. 2. Model for bubble columns operating in the heterogeneous flow regime.

## 2. Development of CFD model

Our approach for modeling purposes is to assume that in the heterogeneous flow regime, we have two distinct bubble classes: "small" and "large" (see Fig. 2). The small bubbles are either spherical or ellipsoidal in shape, depending the physical properties of the liquid [17]. The large bubbles fall into the spherical cap regime. In conformity with the model of Krishna and Ellenberger [2] and Krishna et al. [4] we assume that the superficial gas velocity through the small bubble phase corresponds to that at the regime transition point, $U_{trans}$. The transition velocity can be estimated using the Reilly et al. [18] correlation, or can be provided as model input.

For each of the three-phases shown in Fig. 2, the volume-averaged mass and momentum conservation equations in the Eulerian framework are given by:

$$\frac{\partial(\varepsilon_k \rho_k)}{\partial t} + \nabla \cdot (\rho_k \varepsilon_k \boldsymbol{u}_k) = 0 \tag{1}$$

$$\frac{\partial(\rho_k \varepsilon_k \boldsymbol{u}_k)}{\partial t} + \nabla \cdot (\rho_k \varepsilon_k \boldsymbol{u}_k \boldsymbol{u}_k - \mu_k \varepsilon_k (\nabla \boldsymbol{u}_k + (\nabla \boldsymbol{u}_k)^{\mathrm{T}})) = -\varepsilon_k \nabla p + \boldsymbol{M}_{kl} + \rho_k \boldsymbol{g} \tag{2}$$

where $\rho_k$, $\boldsymbol{u}_k$, $\varepsilon_k$ and $\mu_k$ represent, respectively, the macroscopic density, velocity, volume fraction and viscosity of the $k$th phase, $p$ is the pressure, $\boldsymbol{M}_{kl}$, the interphase momentum exchange between phases $k$ and $l$ and $\boldsymbol{g}$ is the gravitational acceleration.

The momentum exchange between either bubble phase (subscript b) and liquid phase (subscript L) phases is given by:

$$\boldsymbol{M}_{\mathrm{L,b}} = \frac{3}{4}\rho_{\mathrm{L}} \frac{\varepsilon_{\mathrm{b}}}{d_{\mathrm{b}}} C_{\mathrm{D}} (\boldsymbol{u}_{\mathrm{b}} - \boldsymbol{u}_{\mathrm{L}}) |\boldsymbol{u}_{\mathrm{b}} - \boldsymbol{u}_{\mathrm{L}}| \tag{3}$$

The liquid phase exchanges momentum with both the "small" and "large" bubble phases. No interchange between the "small" and "large" bubble phases has been included in the present model and each of the dispersed bubble phases exchanges momentum only with the liquid phase. The interphase drag coefficient is calculated from equation:

$$C_{\mathrm{D}} = \frac{4}{3} \frac{\rho_{\mathrm{L}} - \rho_{\mathrm{G}}}{\rho_{\mathrm{L}}} g d_{\mathrm{b}} \frac{1}{V_{\mathrm{b}}^2} \tag{4}$$

where $V_{\mathrm{b}}$ is the rise velocity of the appropriate bubble population. We have only included the drag force contribution to $\boldsymbol{M}_{\mathrm{L,b}}$, in keeping with the works of Sanyal et al. [8] and Sokolichin and Eigenberger [9]. The added mass and lift forces have been ignored in the present analysis.

For the continuous, liquid phase, the turbulent contribution to the stress tensor is evaluated by means of $k$–$\varepsilon$ model, using standard single-phase parameters $C_\mu = 0.09$, $C_{1\varepsilon} = 1.44$, $C_{2\varepsilon} = 1.92$, $\sigma_k = 1$ and $\sigma_\varepsilon = 1.3$. No turbulence model is used for calculating the velocity fields inside the dispersed "small" and "large" bubble phases.

For the small bubbles the interphase drag coefficient is calculated from [17]:

$$C_{\mathrm{D}} = \tfrac{2}{3}\sqrt{\mathrm{E\ddot{o}}} \tag{5}$$

with:

$$\mathrm{E\ddot{o}} = \frac{g(\rho_{\mathrm{L}} - \rho_{\mathrm{G}}) d_{\mathrm{b}}^2}{\sigma} \tag{6}$$

where $d_{\mathrm{b}}$ is the equivalent diameter of the bubbles. For a single bubble rising in a quiescent liquid, the rise velocity $V_{\mathrm{b0}}$ can be calculated from the drag coefficient:

$$V_{\mathrm{b0}} = \sqrt{\frac{(\rho_{\mathrm{L}} - \rho_{\mathrm{G}}) g}{(3/4)(C_{\mathrm{D}}/d_{\mathrm{b}})\rho_{\mathrm{L}}}} \tag{7}$$

The calculations of the single bubble rise velocity $V_{\mathrm{b0}}$ using Eqs. (5)–(7) compare very well with the rise velocity of single air bubbles in water [19] (see Fig. 3(a)).

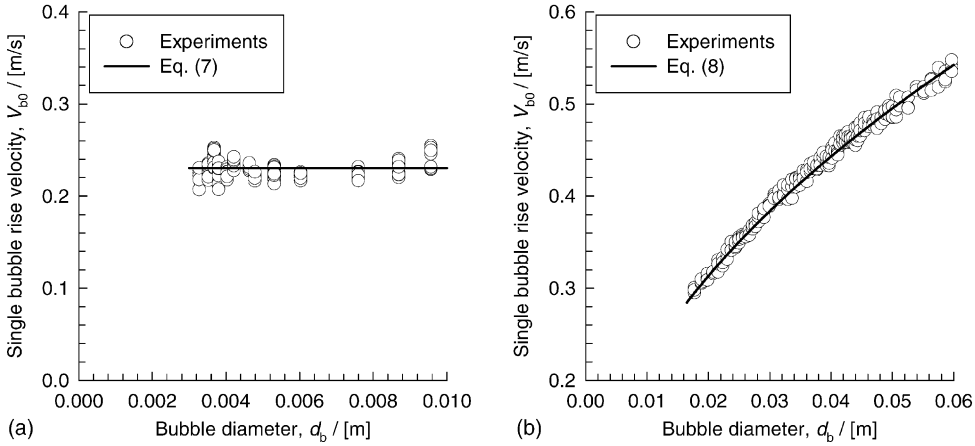


Fig. 3. Experimental data on single bubble rise velocity as a function of bubble diameter [19], compared with predictions of the drag model adopted in this work for (a) small bubbles and (b) large bubbles.

We note that the rise velocity is practically independent of the bubble size in the 3–8 mm range. For the simulations reported here, we choose a small bubble diameter $d_b = 5$ mm.

For values of Eö $> 40$ (for air–water system, this corresponds to bubble sizes larger than 17 mm), bubbles assume a spherical cap shape. The rise velocity of spherical cap bubbles is given by the classic Davies and Taylor [20] relationship:

$$V_{b0} = \sqrt{gd_b/2} = 0.71\sqrt{gd_b} \quad (8)$$

The calculations of the single bubble rise velocity $V_{b0}$ using Eq. (8) compare very well with the rise velocity of single air bubbles in water [19] in the 17–60 mm size range (see Fig. 3(b)).

The drag coefficient for these large bubbles is given by:

$$C_D = \frac{8}{3} \quad (9)$$

In the simulations reported below, a large bubble diameter of 20 mm was used.

A commercial CFD package CFX, versions 4.2 and 4.4, of AEA Technology, Harwell, UK, was used to solve the equations of continuity and momentum. This package is a finite volume solver, using body-fitted grids. The grids are non-staggered and all variables are evaluated at the cell centers. An improved version of the Rhie–Chow algorithm [21] is used to calculate the velocity at the cell faces. The pressure–velocity coupling is obtained using the SIMPLEC algorithm [22]. For the convective terms in Eqs. (1) and (2), hybrid differencing was used. A fully implicit backward differencing scheme was used for the time integration.

Simulations were carried out for bubble columns of 0.1, 0.38 and 1 m diameter with the air–water system, operating at superficial gas velocities in the range $U = 0.01$–$0.08$ m/s. The physical properties used in the simulations are summarized in Table 1. From the Reilly et al. correlation [18], it was determined that the superficial gas velocity at the regime transition point for air–water $U_{trans} = 0.034$ m/s; this is also the value of the regime transition velocity for the experimental data shown in Fig. 1. For air—water operation at $U < 0.034$ m/s, homogeneous bubbly flow regime was taken to prevail. Therefore, only two phases—small bubbles and liquid—are present. For

Table 1
Properties used in the CFD simulations

| | Liquid (water) | Gas (air) |
|---|---|---|
| Viscosity, $\mu$ (Pa s) | $1 \times 10^{-3}$ | $1.7 \times 10^{-5}$ |
| Diffusivity, $Đ$ ($m^2$/s) | $1 \times 10^{-9}$ | $1.0 \times 10^{-5}$ |
| Density, $\rho$ (kg/$m^3$) | 998 | 1.3 |
| Interphase mass transfer coefficient, $k_L$ (m/s) | 0.0004 | 0.0004 |
| Henry coefficient, $H$ | 0.05 | 0.05 |
| Surface tension, $\sigma$ (N/m) | 0.073 | 0.073 |

Table 2
Details of computational grids for the three columns

| Column diameter (m) | Total column height (m) | Observation height (m) | Number of cells in radius | Number of cells in height | Total number of cells |
|---|---|---|---|---|---|
| 0.10 | 1.6 | 1.0 | 15 | 80 | 1200 |
| 0.38 | 2.5 | 1.9 | 38 | 125 | 4750 |
| 1.00 | 7.0 | 4.5 | 50 | 350 | 17500 |

churn-turbulent operation at $U > 0.034$ m/s, the complete three-phase model was invoked. Following the model of Krishna and Ellenberger [2], we assume that in the churn-turbulent flow regime the superficial gas velocity through the small bubble phase is $U_{\text{trans}} = 0.034$ m/s (see Fig. 2). The remainder of the gas ($U - U_{\text{trans}}$) was taken to rise up the column in the form of large bubbles. This implies that at the distributor, the "large" bubbles constitute a fraction $(U - U_{\text{trans}})/U$ of the total incoming volumetric flow, whereas the "small" bubble constitute a fraction ($U_{\text{trans}}/U$) of the total incoming flow.

The simulations were carried out using axi-symmetric 2D grids; the grid details are summarized in Table 2. The small bubbles were injected uniformly over the inner 80% of the bottom patch. The large bubbles were injected uniformly over the inner 60% of the bottom patch. A pressure boundary condition was applied to the top of the column. A standard no-slip boundary condition was applied at all walls. The time stepping strategy used in all simulations was 100 steps at $5 \times 10^{-5}$ s, 100 steps at $1 \times 10^{-4}$ s, 100 steps at $5 \times 10^{-4}$ s, 100 steps at $1 \times 10^{-3}$ s, 200 steps at $3 \times 10^{-3}$ s, 1400 steps at $5 \times 10^{-3}$ s, and the remaining steps until steady state is achieved at $1 \times 10^{-2}$ s. For each run, the hydrodynamics were solved first, in a dynamic approach, until steady state was reached. Steady state was indicated by a situation in which all of the variables remained constant.

The steady state results of a hydrodynamic run were used to start a dynamic mass transfer run in which the hydrodynamic equations were not being solved; the hydrodynamic steady state was maintained throughout a mass transfer run. Initially, liquid, small bubbles and large bubbles were assumed to contain zero concentration of the transferring component or tracer. At the start of the mass transfer run, small and large bubbles are flowing into the simulation domain containing a tracer concentration of unity (arbitrary units). The following equations are solved for the mass tracer:

$$\frac{\partial}{\partial t}\varepsilon_k \rho_k C_k + \nabla \cdot (\varepsilon_k \rho_k \boldsymbol{u}_k C_k - Đ_k \varepsilon_k \rho_k \nabla C_k) = \rho_k F_{kl} \tag{10}$$

Here, $C_k$ is the concentration of mass tracer in phase $k$, $Đ_k$ the diffusion coefficient of mass tracer in phase $k$ and $F_{kl}$ the flux of mass tracer between phases $k$ and $l$ (a.u./s). The flux $F_{\text{GL}}$ for liquid phase L and gas phase G was defined as:

$$F_{\text{GL}} = k_{\text{L}} a (H C_{\text{G}} - C_{\text{L}}) = k_{\text{L}} a (C_{\text{L}}^* - C_{\text{L}}) \tag{11}$$

Here, $k_{\text{L}}$ is the mass transfer coefficient (m/s) and $H$ the Henry coefficient for the mass tracer. The relative surface area $a$ ($\text{m}^2/\text{m}^3$) was calculated for both large and small bubble phases by:

$$a = \frac{6\varepsilon_k}{d_{\text{b},k}} \tag{12}$$

No flux was defined between the large and small bubble phases: mass transfer from either gas phase to the other had to take place through the liquid phase. For the inlets of gas, concentration of mass tracer was explicitly set to unity. No liquid enters or leaves the system. To ensure this, the boundary condition of liquid tracer concentration at the gas inlets and at the outlet were set equal to the concentration directly inside the system for each time step and iteration. No flux of mass tracer was allowed through the walls. Time steps of 1.0 s were taken, until the tracer concentrations in the system attained steady state. Typically, 500 s was sufficient time for the 0.1 m diameter column, 1000 s was sufficient for the 0.38 m diameter column and 2500 s was more than sufficient for the 1.0 m diameter column.

The simulations were carried out on Silicon Graphics Power Indigo workstations with a 75 MHz R8000 processor, a Silicon Graphics Power Challenge with

6 200 MHz R10000 processors or a Windows NT pc with a single Pentium Celeron processor running at 500 MHz. Each hydrodynamic simulation took a time ranging from half a day to a several days, depending on the machine used and the column diameter. Each mass transfer run was completed within a several hours, up to a day.

Further computational details of the model and simulations, along with animations, are available on our web site: http://www.ct-cr4.chem.uva.nl/regimes/.

## 3. Simulation results

To start with, let us examine the influence of column diameter on the hydrodynamics and mass transfer for operation in the *homogeneous* flow regime. A typical transience of the gas and liquid velocities, at the centre of the column, are shown in Fig. 4(a) for operation at $U = 0.02$ m/s for the three columns. Steady state is reached within about 5000 time steps for the 0.1 and 0.38 m diameter columns, whereas the 1 m diameter column requires 10,000 time steps to attain steady state. After the column hydrodynamics has been allowed to reach steady state, the mass transfer run is activated by stepping up the inlet gas concentration to a concentration of 1 a.u. and monitoring the liquid phase concentration in the column at all positions as a function of time. For all the simulations carried out in the study, the tracer concentration in the liquid phase, at any moment of time, could be considered to be spatially uniform. In other words, from a mass transfer point of view the liquid phase can be considered to be well-mixed. The spatially averaged liquid concentration, normalized with respect to the equilibrium concentration ($C_L^*$) is plotted in (Fig. 2) as a function of time $t$. We note that the dynamics of uptake of tracer in the liquid slows down with increasing column diameter. The uptake dynamics for a well-mixed liquid phase is described by [23]:

$$(1-\varepsilon)\frac{dC_L}{dt} = k_L a(C_L^* - C_L) \tag{13}$$

Eq. (13) can be integrated with the following initial and final conditions:

$$C_L = 0, \quad t = 0; \qquad C_L = C_L^*, \quad t \to \infty \tag{14}$$

to obtain

$$\frac{C_L}{C_L^*} = 1 - \exp\left(-\frac{k_L a}{1-\varepsilon}t\right) \tag{15}$$

The continuous lines in Fig. 4(b) have been drawn using Eq. (15) and with fitted values of $k_L a$, using column-average values of $\epsilon$ from the simulation. The fitted $k_L a$ values for the three columns of 0.1, 0.38 and 1.0 m diameter are, respectively, 0.027, 0.0197 and

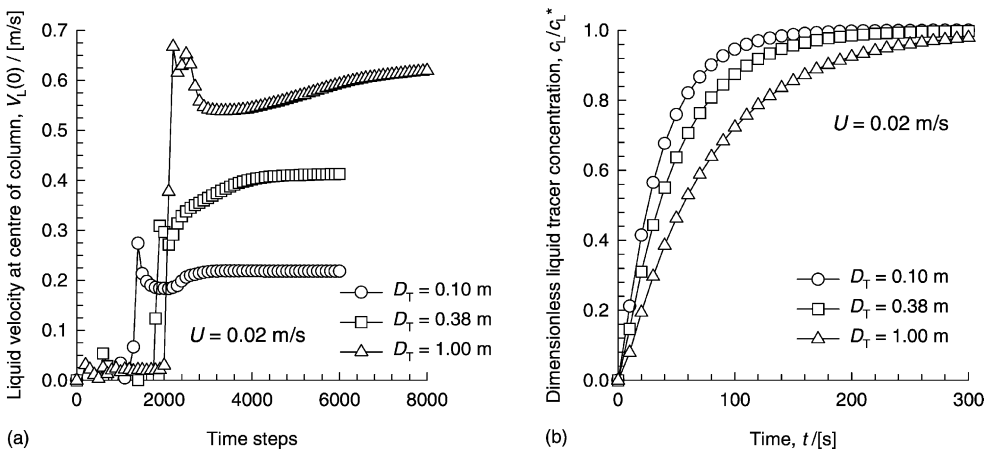


Fig. 4. Transient approach to steady state in the bubble columns of 0.1, 0.38 and 1.0 m diameter. (a) Approach to hydrodynamic steady state for $U = 0.02$ m/s. Animations can be viewed on the web-site: http://www.ct-cr4.chem.uva.nl/regimes/. (b) Dynamics of uptake of tracer in the liquid phase for operation at $U = 0.02$ m/s. The continuous lines in (b) have been drawn using Eq. (15) with fitted $k_L a$ values of 0.027, 0.0197 and 0.0125 $s^{-1}$.

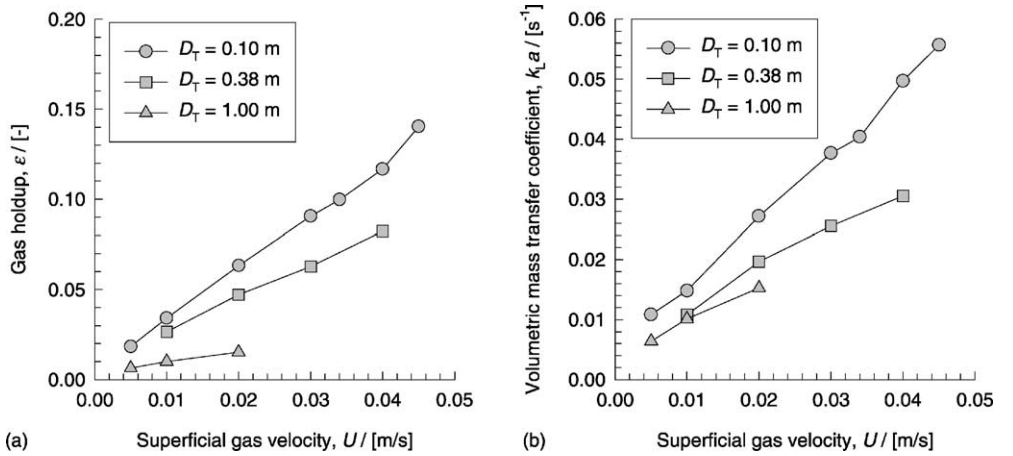


Fig. 5. Influence of column diameter on gas holdup $\varepsilon$ (a) and volumetric mass transfer coefficient $k_La$ (b) for operation in the homogeneous flow regime in the three columns of 0.1, 0.38 and 1 m diameter. Note that in these simulations the dispersion is considered to be made up of 5 mm small bubbles for the whole range of superficial gas velocities $U$.

$0.0125\,s^{-1}$, underlining the strong influence of column diameter on the mass transfer. Simulation results for a range of superficial gas velocities $U$, assuming homogeneous flow regime prevails (dispersion consisting of 5 mm sized small bubbles) are presented in Fig. 5. The strong influence of $D_T$ on $\varepsilon$ and $k_La$ is evident. This aspect has hitherto not been emphasized in the literature.

It is interesting to note in Fig. 5 that the trend in $k_La$ values mirrors the trend in the $\varepsilon$ values. In other words, the reason for the decrease in the $k_La$ with scale must be sought in the corresponding decrease in the gas holdup. In order to gain insight into the scale dependence, let us consider the radial distribution of liquid velocity $V_L(r)$ and gas holdup $\varepsilon(r)$ for $U = 0.02$ m/s; see Fig. 6. We note that with increasing column diameter the liquid circulations become increasingly strong. Such increasing liquid circulations have the tendency to speed up the bubbles in the central core, and thereby reducing gas phase residence time and holdup and, consequently, the mass transfer.

Let us now focus on the influence of *flow regimes* on gas holdup and mass transfer. Simulation results for the average gas holdup (filled circles) for the 0.1

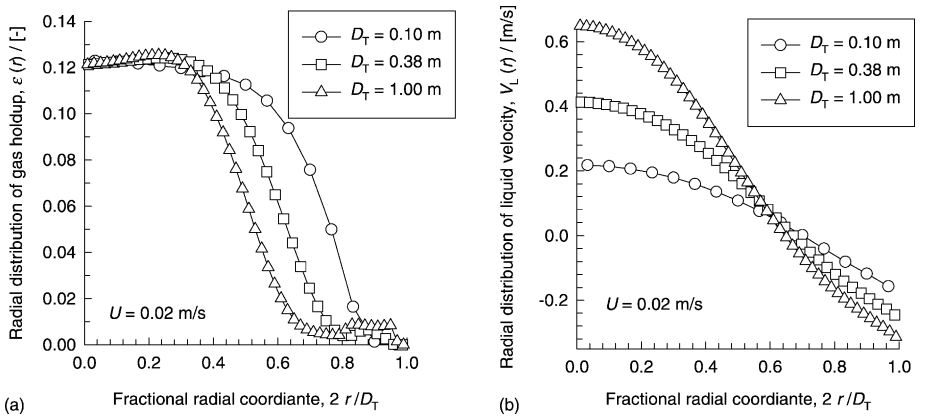


Fig. 6. Radial distribution of gas holdup $\varepsilon(r)$ (a) and liquid velocity $V_L(r)$ (b) for operation at $U = 0.02$ m/s in the three columns of 0.1, 0.38 and 1 m diameter.

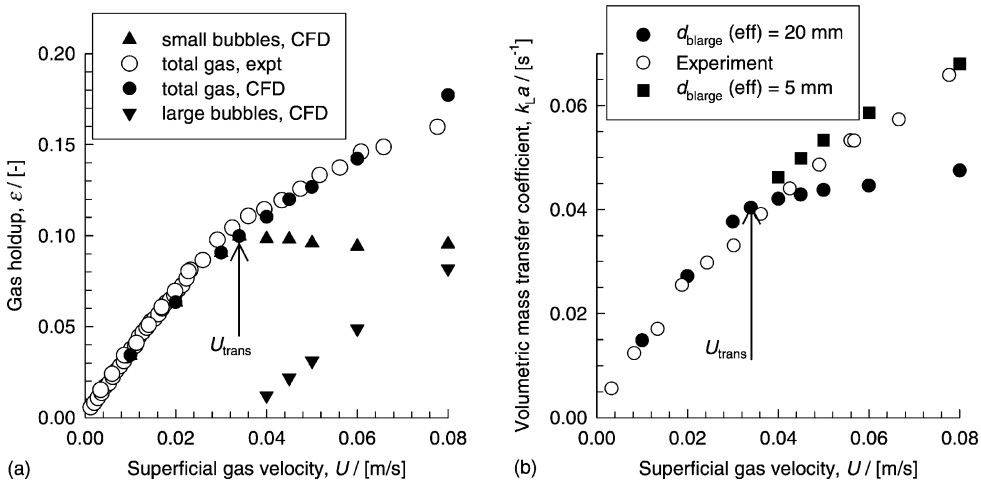


Fig. 7. (a) Cross-section area averaged gas holdup as a function of the superficial gas velocity $U$ for the 0.1 m diameter column. The holdup of total gas, small and large bubbles obtained from CFD are shown by the filled symbols. The open symbol refers to the experimentally determined values. (b) Volumetric mass transfer coefficient as a function of $U$. The filled circles are obtained from CFD taking the effective area of transfer from large bubbles to correspond to 20 mm sized bubbles. The filled squares are obtained from CFD taking the effective area of transfer from large bubbles to correspond to 5 mm sized bubbles shown by the filled symbols. The open circles refer to experimentally determined values.

m diameter column for a range of $U$ values from 0.01 to 0.08 m/s, taking the regime transition velocity $U_{trans} = 0.034$ m/s, are shown in Fig. 7(a). Also plotted in Fig. 7(a) are the values of the small (filled triangles) and large (filled inverted triangles) bubble holdups. In the heterogeneous flow regime, the small bubble holdup attains a constant value, equal to the holdup at the regime transition point, $\varepsilon_{trans}$. This assumption is basic to the model of Krishna and Ellenberger [2] for prediction of the estimation of the total gas holdup in the heterogeneous flow regime. We also note a sharp change in the slope of the $\varepsilon$ versus $U$ curve at $U = U_{trans}$; this is consistent with experimental data obtained in a 0.1 m diameter (also in Fig. 7(a)). The agreement with the experimental gas holdup data confirms the assumption made in the CFD simulations with respect to $U_{trans}$ and the assumed size of the small and large bubbles, 5 and 20 mm, respectively.

The CFD calculations for $k_La$ (indicated by the filled circles) are compared with the experimental values (obtained in 0.1 m diameter air–water column using the oxygen absorption technique [23]) in Fig. 7(b). We note that the agreement in the $k_La$ values in the homogeneous flow regime ($U < U_{trans}$) is very good. However, in the heterogeneous flow regime ($U > U_{trans}$) the CFD simulations predict much lower $k_La$ values than observed in the experiments. The reason for this discrepancy can be found in the experimental work of De Swart et al. [3]. The large bubbles suffer frequent coalescence and break-up at frequencies of the order of 5–20 $s^{-1}$, depending on the size. As a result the effective bubble diameter for mass transfer, is reduced significantly [3]. To match the experimental values of $k_La$ in the heterogeneous flow regime, the effective transfer area for large bubbles have to be increased. The filled squares show the CFD calculations in which the large bubble interfacial area is assumed to correspond to that of 5 mm bubbles, but retaining the hydrodynamics corresponding to 20 mm bubbles. The agreement with experimental data is much improved with this assumption.

## 4. Conclusions

We have developed a CFD model to describe the hydrodynamics and mass transfer of an air–water bubble column operating in both homogeneous and heterogeneous flow regimes. In the homogeneous flow regime, both gas holdup $\varepsilon$ and mass transfer

coefficient $k_L a$ show a strong reduction with column diameter; this is due to increased liquid circulations that tend to accelerate the bubbles in the central core, reducing gas–liquid contact time.

The small bubble holdup is practically constant in the heterogeneous flow regime and its value corresponds to that at the regime transition point (see Fig. 7(a)). Our CFD simulations verify this basic assumption of the Krishna–Ellenberger [2] model. The CFD simulations for mass transfer show that in the heterogeneous flow regime we must take account of the enhancement in the mass transfer due to frequent coalescence and break-up [3].

## Acknowledgements

The Netherlands Organisation for Scientific Research (NWO) is gratefully acknowledged for providing financial assistance in the form of a "programmasubsidie" for development of novel concepts in reactive separations technology.

## References

[1] W.D. Deckwer, Bubble Column Reactors, Wiley, New York, 1992.
[2] R. Krishna, J. Ellenberger, AIChE J. 42 (1996) 2627–2634.
[3] J.W.A. de Swart, R.E. van Vliet, R. Krishna, Chem. Eng. Sci. 51 (1996) 4619–4629.
[4] R. Krishna, J. Ellenberger, S.T. Sie, Chem. Eng. Sci. 51 (1996) 2041–2050.
[5] H.A. Jakobsen, B.H. Sannaes, S. Grevskott, H.F. Svendsen, Ind. Eng. Chem. Res. 36 (1997) 4050–4072.
[6] J.B. Joshi, Chem. Eng. Sci. 56 (2001) 5893–5933.
[7] Y. Pan, M.P. Dudukovic, M. Chang, Chem. Eng. Sci. 54 (1999) 2481–2489.
[8] J. Sanyal, S. Vasquez, S. Roy, M.P. Dudukovic, Chem. Eng. Sci. 54 (1999) 5071–5083.
[9] A. Sokolichin, G. Eigenberger, Chem. Eng. Sci. 54 (1999) 2273–2284.
[10] R. Krishna, J.M. van Baten, M.I. Urseanu, Chem. Eng. Technol. 24 (2001) 451–458.
[11] R. Krishna, M.I. Urseanu, J.M. van Baten, J. Ellenberger, Chem. Eng. Sci. 54 (1999) 4903–4911.
[12] R. Krishna, J.M. van Baten, M.I. Urseanu, Chem. Eng. Sci. 55 (2000) 3275–3286.
[13] R. Krishna, J.M. van Baten, Chem. Eng. Sci. 56 (2001) 6249–6258.
[14] J.M. van Baten, R. Krishna, Chem. Eng. Sci. 56 (2001) 503–512.
[15] R. Krishna, J.M. Van Baten, Chem. Eng. Res. Des. 79 (2001) 283–309.
[16] R. Krishna, J.M. van Baten, M.I. Urseanu, J. Ellenberger, Chem. Eng. Sci. 56 (2001) 537–545.
[17] R. Clift, J.R. Grace, M.E. Weber, Bubbles, Drops and Particles, Academic Press, San Diego, 1978.
[18] I.G. Reilly, D.S. Scott, T.J.W. De Bruijn, D. MacIntyre, Can. J. Chem. Eng. 72 (1994) 3–12.
[19] R. Krishna, M.I. Urseanu, J.M. van Baten, J. Ellenberger, Int. Commun. Heat Mass Transfer 26 (1999) 781–790.
[20] R.M. Davies, G.I. Taylor, Proc. R. Soc. London, Ser. A 200 (1950) 375–390.
[21] C.M. Rhie, W.L. Chow, AIAA J. 21 (1983) 1525–1532.
[22] J. van Doormal, G.D. Raithby, Numer. Heat Transfer 7 (1984) 147–163.
[23] H.M. Letzel, J.C. Schouten, R. Krishna, C.M. van den Bleek, Chem. Eng. Sci. 54 (1999) 2237–2246.